Analysis of Square Tube Bending by MOS Bending Method

Makoto Murata and Takashi Mochizuki

Department of Mechanical and Control Engineering
The University of Electro – Communications, Tokyo 182, Japan

Abstract

A new flexible CNC bending machine, which was named the MOS bending machine, has been invented by the authors. When square tubes are passed into the guide cylinder and the bending die, they are bent by shifting the relative position of the bending die. The bending radii are controlled by the relative distance between the die and the square tube. The bending angle is controlled by the penetrating square tube length. This CNC bending machine which can bend square tubes using the MOS bending method has been built. The effects of the penetration force, the bending force, bending moment and the bending radius are presented on such bending conditions as changing the relative distance between the die and the square tube. The analytical values are compared with and shown to agree with the experimental ones.

Keywords: *metal forming, tube forming, MOS bending, bending moment, bending radius.*

1 Introduction

Tubes are used to reduce the weight of industrial parts, because tubes have height rigidity as compared with weight. Many tubes are bent, when they are employed as industrial parts, therefore there are many bending methods such as draw bending, press bending, stretch bending and others. The conventional bending methods are not suited for short production runs in various of sizes and shapes.

These methods need many bending dies which are required for the variety of bending radii and tube diameters. Therefore, the square tube is bent by using the MOS bending method, from which it is possible for many varied bending radii to be obtained, and we tried to make this bending method clear.

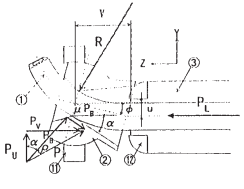

Fig.1 Principal parts of the bending machine.

2 CNC Bending

2.1 Bending Mechanism

The principal parts of the bending mechanism are

shown in **Fig.1**. The relative distance between the center line of guide cylinder ③ and the center line of bending die ② is called offset **u**. A square tube ① is passed into the die from guide cylinder by the penetrating force $\mathbf{P}_L$, then the square tube is bent at bending radius **R** as shown in **Fig.1**. On this machine, the approach **V** is a constant value. The bending force $\mathbf{P}_U$ depends on the magnitude of offset **u**. When the square tube is bent, the bending moment $\mathbf{M}(= P_L * u + P_U * V)$ operates on it.

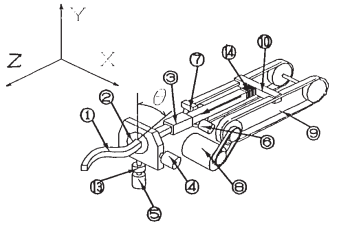

①Square tube,
②Bending die,
③Guide cylinder,
④AC serve for control of X axis,
⑤AC serve for control of Y axis,
⑥Rotary encoder for measurement of forward tube length, ⑦Approach switch,
⑧Motor for forming of tube,
⑨Chain for forwarding of tube,
⑩Plate for forwarding of tube,
⑪Spherical bearing,
⑫Jig for control of die inclination,
⑬Load cell for penetration load,
⑭Load cell for bending load

Fig.2 **MOS** bending machine.

2.2 Process of MOS bending

The MOS bending machine is shown in **Fig.2**. This bending machine can bend the tube by controlling the position of the die using a micro computer and AC servo motors. The bending is carried out as follows. When the square tube ① is inserted into the guide cylinder ③, the motor for forming of tube⑧ for control of Z axis is activated to enter it into the bending die ②. When an approach switch⑦ senses the top of the square tube, and the bending die is moved continuously by the AC servo motors for X and Y axes, the bending is begun. The bending die is moved in only the Y axis in this study.

2.3 Analysis of MOS Bending

At first, the assumption about analysis of MOS bending method is shown as follows. The bending force of the this analysis is only the vertical force to the central axis. The square tube is not flattened after bending and the cross section is vertical to the neutral surface. The relationship between the stress and strain of the square tube is represented by the following equations.

$$\text{Elastic region}: \quad \sigma = E\,\varepsilon \tag{1}$$

$$\text{Elastic plastic}: \quad \frac{\sigma}{E} + \left(\frac{\sigma - \sigma_e}{F}\right)^{\frac{1}{n}} = \varepsilon \tag{2}$$

σ :Stress
σ_c :0.2% Yield stress
E: Young's modulus
ε :Strain **n** and **F** :Material value

Dimensions of the square tube **H** and the bending radius **R** are shown in Fig.3. It is assumed that the neutral axis is moved from a neutral surface to the outside $\mathbf{Y_0}$. The strain distribution is shown in Fig.3(b) and the stress distribution corresponding with strain distribution is shown in Fig.3(c). The moment dM and penetrating force dP_L which exist at minute part y distance from the center of tube are given as follows in equation (3) and (4).

$$\int dM = \int \sigma y dA \qquad (3)$$

$$\int dP_L = \int \sigma \, dA \qquad (4)$$

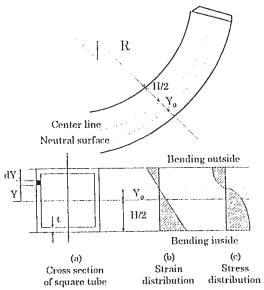

Fig.3 Stress and strain distributions of cross section.

Since the neutral surface is moved **Y** to the outside, strain ε which exists at the part is represented by equation (5) as follows.

$$\varepsilon = \frac{y - y_o}{R + \frac{H_0}{2} + y_0} \qquad (5)$$

The geometric bending radius is represented by equation (6) as follows.

$$R = \frac{V^2 + u^2 - H_0 u}{2u} \qquad (6)$$

The equilibrium of forces which is added to the square tube is shown in **Fig.1**. The equilibrium equation of the penetrating force and the bending force is given as follows in equations (7) and (8).

$$P_L = P_U \tan(\alpha + \rho) \qquad (7)$$

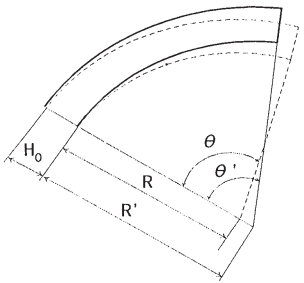

Fig.4 Bending radii at loading and unloading.

$$\rho = \tan^{-1}\mu \qquad (8)$$

α : inclining angle of the bending die

μ : coefficient of friction

The $\mathbf{M}_U$ and $\mathbf{M}_L$ are given as following equations (9) and (10). Equation (11) is approved by $\mathbf{M}_U$ and $\mathbf{M}_L$ and the moment $\mathbf{M}$ equals the moment which is calculated from equation(3).

$$M_U = P_U V \qquad (9)$$

$$M_L = P_L u \qquad (10)$$

M is represented by equation (11) from equations (9) (10).

$$M = M_U + M_L \qquad (11)$$

$\mathbf{P}_L$, $\mathbf{P}_U$, $\mathbf{M}_U$ and $\mathbf{M}_L$ are solved by the 9 previous equations. The adequate $\mathbf{R}$ is assumed as a first step. The values of $\mathbf{Y}_0$ and ε are calculated according to this assumption. In addition to $\mathbf{Y}_0$ and ε, σ is calculated with ε. Using the calculated σ and former 9 equations, $\mathbf{dM}$ and $\mathbf{P}_L$ are calculated by equations (3) and (4), and $\mathbf{M}$ is calculated by equation (12). If these values do not correspond to each other, a new $\mathbf{R}$ is assumed, and then $\mathbf{M}$ and $\mathbf{P}_L$ are recalculated by the same process.

2.4 Analysis of Springback of Bending

The assumption of springback of bending is explained as follows; P and Q show the increase of strain on loading as in equation (12). The residual stress σ_{res} is represented with the stress on unloading as equation (13).

$$\Delta\varepsilon = PY + Q \qquad (12)$$

$$\sigma_{res} = \sigma + E\,\Delta\varepsilon \qquad (13)$$

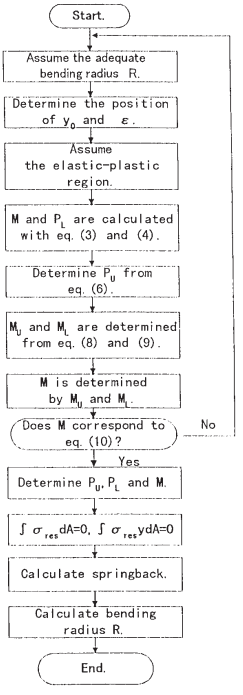

Fig.5 Flow chart of calculation for MOS bending.

The sums of the forces and moment in the axial direction become zero as indicated in equations

(14) and (15). Using two equations, the numbers P and Q are calculated.

$$\int \sigma_{res}\, dA = 0 \qquad (14)$$

$$\int \sigma_{res}\, y dA = 0 \qquad (15)$$

The bending radii at loading and unloading are shown in Fig.4. The bending radii on loading and unloading are composed of incremental nominal strain of loading (ε_A) and unloading (ε_B) of the square tube as indicated in equations (16) on the inside and (17) on the outside.

$$R'\theta = R(1+\Delta\varepsilon_A) \qquad (16)$$

$$(R'+H_0)\theta' = (R+H_0)\theta(1+\Delta\varepsilon_B) \qquad (17)$$

The amount of springback and the bending radii at unloading are able to be calculated in equation (18) as follows.

$$\beta = \frac{\Delta\theta}{\theta} = \frac{(\theta-\theta')}{\theta} = -(R+H_0)P - Q \qquad (18)$$

The bending radius and springback are calculated as shown in Fig.5.

3 Result and Examination

The relationship between the calculated and the experimental values of the penetrating force and the bending force is shown in **Fig.6**. The relationship between the calculated and experimental values of the moment is shown in **Fig.7**. The calculated and the experimental penetrating forces become larger as the offset **u** increases. But both the bending forces become slightly smaller in spite of increasing of the offset **u**. The experimental and calculated bending moments become larger as the offset **u** increase. The tendency of these calculated values agree with the tendency of the experimental values. But there are some differences between the calculated and experimental values. The bending moment is the sum of the penetrating force and the bending force and the calculated values of the bending forces are much larger than the experimental ones. Because the deformation of a cross section is not considered in this calculation. Friction is a big problem in bending analysis.

The relationship between the calculated and the experimental radii at unloading is shown in Fig8. The calculated radii agree with the experimental ones in the range where the offset is large. But the calculated radii do not agree with the experimental ones in the range where the offset is small. The reason for this is; The calculated values of springback are smaller than experimental ones in the range where offset is small.

4.Conclusion

Comparing the calculated and the experimental values, the results are indicated as follows;

The bending moment is combined with the penetrating force and the bending force using the MOS bending method. Both forces (penetrating force and the bending force) and the bending radii are elucidated by calculation and the calculated values almost match the experimental ones without the bending force. The authors expect that this analysis will be useful, if the deformation of a cross section would be considered and the friction problem between the square tube and the bending die would be solved.

Table.1 Material table.

Material	A1050
Height of square tube H_0 (mm)	15
Thickness t(mm)	1.0
Ultimate tensile strength σ (MPa)	75.7
Elongation Δl(%)	32.9
Young's modulus E (GPa)	50.0
Plastic modulus F (MPa)	175.8
Work-hardning exponent n	0.411

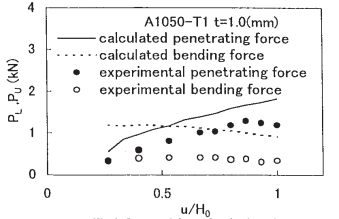

Fig.6 Comparision of calculated and experimental forces.

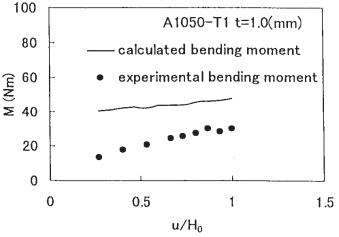

Fig.7 Comparision of calculated and experimental bending moment.

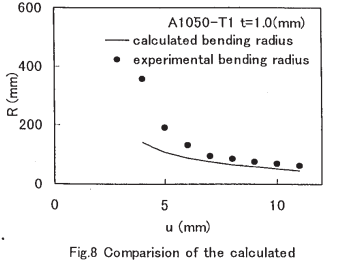

Fig.8 Comparision of the calculated and experimental bending radii.

5 Reference

(1) M.Murata and Y.Aoki: Advanced Technology of Plasticity, 505,(1996).